Journal of Nano Research *Online: 2012-01-11*
ISSN: 1661-9897, Vol. 16, pp 119-130
doi:10.4028/www.scientific.net/JNanoR.16.119

New Approach to Ammonia Synthesis by Catalysis in Magnetic Field

Noorhana Yahya[1,a], Poppy Puspitasari[2,b], Krzysztof Koziol[3,c] and Giuseppe Pavia[4,d]

[1]Department of Fundamental and Applied Science,
[2]Department of Electrical and Electronic Engineering,
Universiti Teknologi PETRONAS,
Bandar Seri Iskandar, 31750, Tronoh, Perak, Malaysia
[3]Department of Materials Science and Metallurgy,
University of Cambridge, Pembroke Street, Cambridge, United Kingdom
[4]Carl Zeiss NTS GmbH, Carl Zeiss
Strasse 56, 73447 Oberkochen, Germany

[a]noorhana_yahya@petronas.com.my (corresponding author), [b]povopivi@gmail.com,
[c]kk292@cam.ac.uk, [d]g.pavia@nts.zeiss.com

Keywords: ammonia synthesis, ferrites, catalysis, sol gel, microreactor, Kjeldahl method

Abstract. Ammonia production is a capital-intensive industry as it requires high temperature (400-500^{o}C) and also high pressure (150-300 bar) for its daily operations. An earnest effort was made to synthese ammonia gas using an in-house designed microreactor. The production of ammonia was carried out in a magnetic field reaction zone, with the reaction temperature of 30°C - 280°C and ambient operation pressure. $Mn_{0.8}Zn_{0.2}Fe_2O_4$ nanoparticles, synthesized using the sol gel method, were used as the catalyst for the ammonia synthesis. XRD confirmed the single phase ferrites and FESEM images revealed nanofibre-like morphology when sintered at 700^{o}C in argon gas. Electron diffraction was performed using HRTEM and obtained diffraction patterns confirmed the crystal structure of the catalyst. By using the Kjeldahl method it was found that the reaction carried out in 1 Tesla magnetic field gave approximately 46% ammonia yield. The proposed new method could be appealing for ammonia manufacturers due to highly economical implication which may offer urea producers a potential contender in the competitive market place.

Introduction

A. Ammonia Synthesis

Ammonia (NH_3) is a very important commodity in our life. It can be naturally found in small quantity in our atmosphere. Due to the importance of ammonia particularly as a fertilizer in the agriculture industry, the production rate has been extensively increasing every year. Ammonia is obtained by reacting nitrogen and hydrogen gases in the presence of a catalyst. In most industrial produced ammonia, the catalyst used is magnetite (Fe_3O_4) and the process is known as the Haber-Bosch process. This process requires a high temperature in the range of 300^{o}C to 500^{o}C and a high pressure (150-300 atm) giving approximately 14% ammonia yield [1]. The magnetite will be reduced to iron before any catalytic activity takes place. Iron is one of the transition metals with its d-orbital partially occupied by electrons. Manganese also has a d-orbital which is partially occupied by electrons. Manganese has five unpaired electrons whereas iron has four unpaired electrons hence they are very attractive for magnetic applications [2]. The method currently used to synthesize ammonia was pioneered by Fitz Haber and Carl Bosch. Their approach became a reference for all of the ammonia industries.

For this process, an important part, which determines the success of production in terms of ammonia yield, is the reactor design. In this project, the reactor is filled with an appropriate catalyst and equipped with input and output tubes for the flow of reactant gases. The reactor is also connected with a return tube to ensure that the non reacted gases can flow back to the input part so that the catalytic reaction can be maximized. In order to perform a complete reaction, the environment inside the reactor must be identical with the required environment of the reaction studied. We also propose the catalytic reactions to be conducted in a magnetic reaction zone.
In the conventional ammonia production case, the reactor must be able to operate at high temperature (400-500^{o}C) and pressure (150-300 atm) environments to ensure the reaction can be done successfully [3,4]. Another important parameter that needs to be considered is the appropriate ratio of reactant gas supply. The ratio of hydrogen to nitrogen gases (H_2:N_2) must always be 3:1 according to the stoichiometric ratio as given in the equation below:

$$N_2 + 3H_2 \leftrightarrow 2NH_3$$

The synthesis of ammonia is known as a reversible and exothermic reaction. At high temperature, more nitrogen and hydrogen molecules have sufficient activation energy to overcome the barrier to react (activation energy) therefore the reaction is faster at high temperatures. High temperature means heat is added to the system. Because formation of ammonia is an exothermic reaction, reversible reaction will occur in order to achieve equilibrium reaction producing more reactant than product (ammonia). In order to get as much ammonia as possible, the temperature applied needs to be lowered to ensure the equilibrium position is moved to the right side. With the temperature optimization, higher yield can be produced but the reaction will take a longer time to be completed due to the decrease in reaction rate. Increasing the pressure brings the molecules closer together and induces their chances of hitting and sticking to the surface of the catalyst where they can react. The reaction rate will be increased and the time taken for complete reaction will be shorter. Following the Le Chatelier principle, the forward reaction will be favoured to achieve an equilibrium reaction producing more ammonia with increased pressure [4,5].

Methodology

A. Preparation of manganese zinc ferrite ($Mn_{0.8}Zn_{0.2}Fe_2O_4$) by sol gel method

A stoichiometric mixture of manganese nitrate, $Mn(NO_3)_2{\cdot}4H_2O$; zinc nitrate, $Zn(NO_3)_2{\cdot}6H_2O$; and iron nitrate, $Fe(NO_3)_3{\cdot}9H_2O$ was prepared by dissolving in aqueous solution of 150 mL nitric acid (HNO_3). The solution was stirred for 1 day. The gel-like structure was formed by heating the mixture at 70^{o}C. During the sol to gel transition, the solution viscosity increases gradually at first and finally the overall medium is rapidly converted to a quasi homogeneous solid-like mass, where no concentration gradient is developed. After the formation of the gel, the sample was dried at 110^{o}C in an oven for 24 hours and the dried powder was crushed by using a mortar for 1 hour. Then, a furnace was used to anneal the samples at 700^{o}C, 800^{o}C and 900^{o}C, with a holding time for 4 hours in air. Furthermore, the green powder was sintered at 1000^{o}C and 1100 ^{o}C in an argon atmosphere for 4 hours.

B. Characterization of Nanocatalyst

The as-synthesized nanocatalyst was characterized by X-Ray Diffraction (XRD), Field Emission Scanning Electron Microscopy (FESEM), Energy Dispersive X-ray Spectroscopy (EDX) and High Resolution Transmission Electron Microscopy (HRTEM). XRD was used for the phase identification, level of crystallinity, average crystallite size (Scherrer's formula) and determination of lattice parameters. The FESEM (SUPRA 35VP version) gives the microstructure evaluation on

the sintered powder. Olympus BX41 Horiba Jobin Yvon HR800 Temperature Program Reduction (TPR), TPDRO 1100 series, was used to study the activation energy of the sintered sample $Mn_{0.8}Zn_{0.2}Fe_2O_4$ when it was reduced to the metallic state.

C. Ammonia Synthesis

In the first step of the process the nanocatalyst was loaded inside the reactor chamber. Next, hydrogen gas was introduced into the chamber and set on continuous flow to ensure that the catalyst was maintained in the reduced state. After 1 hour of running the hydrogen gas, the external magnetic field was turned on to magnetize the catalysts. Nitrogen gas was subsequently passed through the reactor chamber for about two hours (Fig. 1).

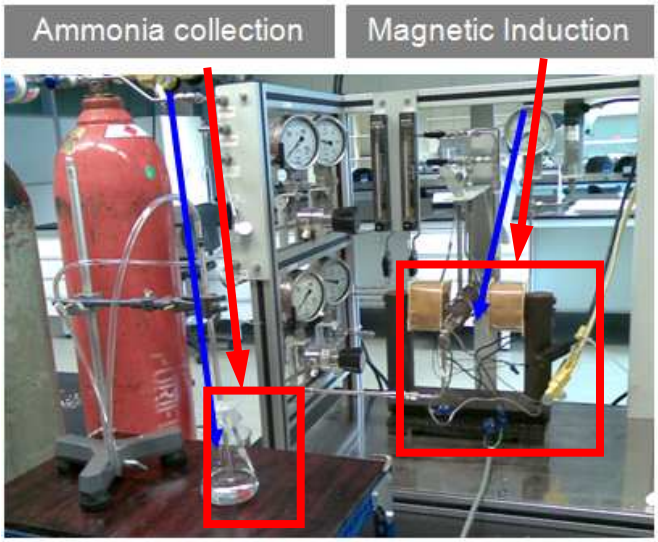

Fig. 1: Ammonia Synthesis Reactor.

The product (ammonia) was collected in a glass beaker filled with 0.1 M HCl to form NH_4Cl (ammonium chloride). Prior to this, TPR studies were performed to understand the reduction profile of the $Mn_{0.8}Zn_{0.2}Fe_2O_4$ catalyst. The product was then analyzed by Fourier-Transform Infrared Spectroscopy (FTIR). Titration (Kjeldahl method) was used to quantify the amount of ammonia synthesised [6,7,8]. The titration approach is shown below:

$$HCl_{reaction} + NH_3 \rightarrow NH_4Cl$$

$$NaOH + HCl_{excess} \rightarrow NaCl + H_2O$$

$$HCl_{total} = HCl_{reacted} + HCl_{excess}$$

Results and Discussion

A. X-Ray Diffraction

X-ray diffraction (XRD) analysis as performed on all the samples using a Philips X-Ray Diffractometer (with CuKα, λ = 1.5418 Å). The reflections were acquired from 10° to 80° (2θ) with the step size of 0.02°. The X-Ray diffraction patterns of the $Mn_{0.8}Zn_{0.2}Fe_2O_4$ catalyst sintered for 4 hours at 700°C, 800°C, 900°C, 1000°C and 1100°C are shown in Fig. 2.

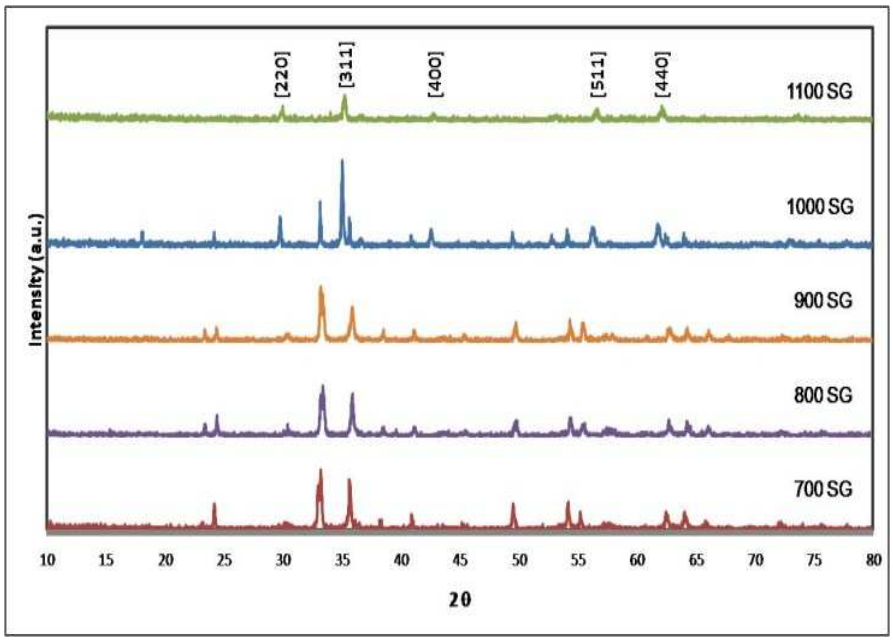

Fig. 2: X-Ray Diffraction pattern for $Mn_{0.2}Zn_{0.8}Fe_2O_4$ annealed at 700°C, 800°C, 900°C, 1000°C and 1100°C for 4 hours.

The unit cell size and geometry were determined from the angular positions of the diffraction peaks, whereas the arrangement of atoms within the unit cell was associated with the relative intensities of these peaks. The diffraction patterns of manganese zinc ferrite powders show an evolution in the crystallization with increasing annealing temperature. The highest peak intensity is observed for the (311) plane, which corresponds to the $MnFe_2O_4$ [9]. It should be noted that the major peak only appeared when the powder was sintered at 1000ºC. This signified that the annealing process had caused atoms to move from its own lattice completely. It is speculated that Zn^{2+} ions occupied the tetrahedral site, Mn^{2+} ions occupied the octahedral site and the Fe^{3+} ions were distributed over both sites [9]. Powder sintered from 700ºC to 1000ºC shows a mixture of hematite and ferrite phase (patterns dominated by hematite), whereas powder sintered at 1100ºC firmly exhibit the spinel ferrite phase only.

Table I. Intensity, FWHM, d-spacing, crystallite size of $Mn_{0.8}Zn_{0.2}Fe_2O_4$ prepared using the sol gel technique, sintered at 700°C, 800°C, 900°C, 1000°C and 1100°C for 4 hours.

Samples	X-Ray Diffraction (Correspond to [311] peaks)					
	FWHM	d-spacing (Å)	Crystallite size (nm)	a	b	c
700 SG	0.39	2.70	21.10	8.4915	8.4915	8.4915
800 SG	0.38	2.68	21.80	8.4915	8.4915	8.4915
900 SG	0.24	2.68	34.10	8.3820	8.3820	8.3820
1000 SG	0.18	2.56	457.90	8.4915	8.4915	8.4915
1100 SG	0.23	2.54	359.09	8.4500	8.4500	8.4500

Table I shows the XRD analysis, including the full width half maximum (FWHM), d-spacing and crystallite size based on the (311) reflection. The diameter of manganese zinc ferrite crystallite is determined using Scherrer's equation:

$$D = \frac{K\lambda}{\beta \cos\theta}$$

where: K = 0.9, λ = 1.5418Å, β = peak FWHM (full width half maximum), θ = peak position.

B. FESEM results

A Field Emission Scanning Electron Microscope (FESEM) was used to identify the surface morphology of nanostructure and dimension of grain size for all powder samples. Ferrites are extremely process-sensitive and hence, microstructure dependent. This is well known. This part discusses the grain size and morphology of all sintered samples.

Fig. 3 (a) shows the nanofiber-like morphology of $Mn_{0.8}Zn_{0.2}Fe_2O_4$. Dimensions of these nanorods are in the range of 62-72 nm. Samples sintered at 800ºC and 900ºC exhibit spherical-like morphologies (Fig. 3 (b) and Fig. 3 (c)) is particularly very unique, and would be an added advantage during reaction due to its large surface area.

$Mn_{0.8}Zn_{0.2}Fe_2O_4$ powder that was sintered at temperature 1000ºC and 1100ºC, respectively show a larger grain size in the range of 417 – 534nm (Fig. 3 (d) and Fig. (e)). It should also be noted that the samples exhibit large grain size and porous structure. The FESEM results are consistent with the crystallite size of the samples. From Table I, the higher sintering temperature shows a bigger crystallite size.

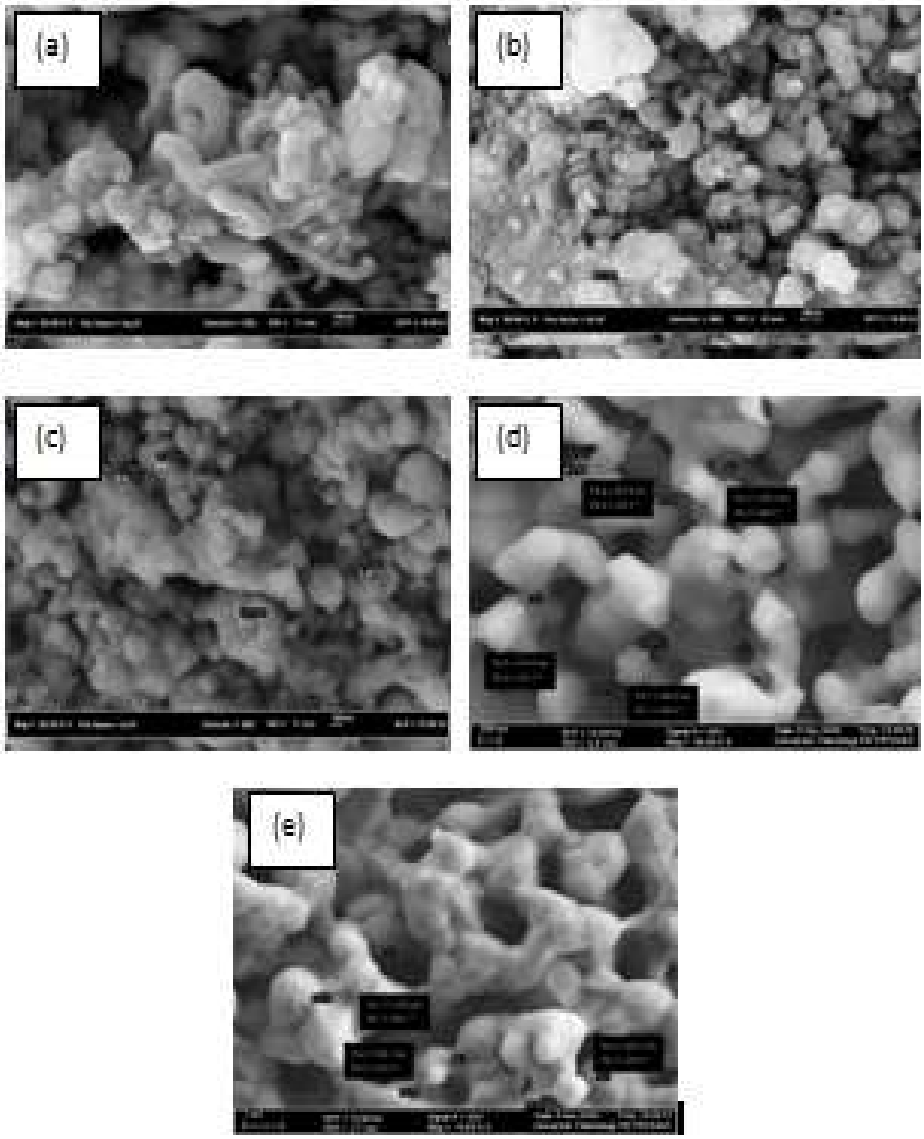

Fig. 3: FESEM morphology of $Mn_{0.8}Zn_{0.2}Fe_2O_4$ at different sintering temperatures (a) 700^{o}C, (b) 800^{o}C, (c) 900^{o}C, (d) 1000^{o}C, and (e) 1100^{o}C.

C. Energy Dispersive X-Ray spectroscopy

Energy Dispersive X-Ray (EDX) spectroscopy data (Table II) indicates the atomic and weight percentage of the corresponding elements; manganese, zinc, iron and oxygen. The results show that the as-synthesized sample has the elements: Mn, Zn, Fe and O. Table II shows the atomic percentage of each element compared to the theoretical value (Mn = 11.42%, Zn = 2.86%, Fe = 28.57%, and O = 57.14%). Standard deviation value for sample 700 SG, sample 800 SG, sample 900 SG and sample 1100 SG show 29.51% - 45.45% difference of the atomic percentage of Mn compared to the theoretical value, while sample 1000 SG shows only 6.39% difference of atomic percentage of Mn compared to the theoretical value. Other research has reported that the formation of manganese ferrite was temperature dependent and well defined manganese ferrite was formed at 1000°C – 1200°C [10].

Table II. Percentage weight and atom $Mn_{0.8}Zn_{0.2}Fe_2O_4$ at different temperatures.

		Mn	Zn	Fe	O
700 SG	Weight %	13.55	7.50	50.01	28.94
	Atomic %	8.05	3.75	29.21	59.00
	Std Deviation %	29.51	31.12	2.24	3.26
800 SG	Weight %	11.06	7.59	48.70	32.66
	Atomic %	6.23	3.59	26.99	63.18
	Std Deviation %	45.45	25.52	5.53	10.57
900 SG	Weight %	17.57	6.59	45.46	30.02
	Atomic%	10.26	3.41	26.12	60.21
	Std Deviation %	10.15	19.23	8.57	5.37
1000 SG	Weight %	19.40	5.04	50.38	25.18
	Atomic %	12.15	2.65	31.04	54.15
	Std Deviation %	6.39	7.34	8.64	5.23
1100 SG	Weight %	24.45	6.26	43.81	25.48
	Atomic %	15.25	3.28	26.89	54.58
	Std Deviation %	33.54	14.68	5.88	4.48

D. Transmission Electron Microscopy

Transmission Electron Microscopy (TEM) analysis has been performed using a ZEISS Libra 200 EFTEM, equipped with in-column energy filter. Images and diffraction patterns have been acquired by zero loss filtering in order to remove inelastically scattered electrons and the diffuse background in the diffraction patterns.

Accelerated electrons as particles, due to their momentum, have wave-like behaviour. The electron beam must also been considered as a plane wave which interacts with the specimen. Compared to photons however, the electrons have a much stronger interaction with matter, due to their electrical charge. This has a very important effect especially on diffraction: when travelling through a

specimen, electrons are usually Bragg-scattered more than once, and peak intensities are changed by this phenomenon, with respect to the single diffraction event occurred by X-rays. For electron diffraction the kinematical theory developed for describing the X Ray diffraction is not completely suitable, and the correct framework is the much more complex Dynamical Theory of Diffraction. Another aspect is that the very small electron wavelength (2 - 4 pm, in most TEMs, depending on the accelerating voltage) allows the probing of very small objects, with a size below the detection limit for photon based techniques. Electron diffraction provides information about the presence of crystalline structure of a sample which may be single crystals of polycrystalline material.

Fig. 4: Bright field image of a crystal agglomerate.

Further analysis of the diffraction pattern can provide information about lattice spacing and crystal symmetry. This is a bright field image which shows an agglomerate of small particles partially lying on the net of a Lacey Carbon Film, and partially protruding into the vacuum (Fig. 4).
The agglomerate of particles is surrounded by an easily recognizable layer of carbon based material, about 10 nm thick, formed by the alcohol in which the particles were dispersed before being collected on the TEM grid.
Enlargement of the image shows the presence of Moiré fringes, which appear when two crystals with different orientation are superimposed along the electron beam path, thus introducing the idea that the material is at least partially crystalline. Increasing the magnification up to lattice resolution is not always the preferred choice, because when particles are oriented to a high index zone axis with respect to the beam, the lattice may not visible because the spacing is beyond the instrument resolution.
Electron diffraction is much less limited in this sense and, especially in the case of polycrystalline materials as is suggested by the bright field TEM image. In Fig. 5 the diffraction pattern, obtained from the area circled in red in the TEM image, is shown. This is the typical diffraction pattern formed from a polycrystalline material, when not so many grains are present in the diffracting area. The sequence of rings radii indicates that the material has a cubic structure. The indexing of the planes is consequently done and the lattice parameter can be calculated to be about 0.85 nm. In fact, for cubic materials, there is a simple relation between the interplanar distance d_{hkl} and the lattice parameter a. This result is consistent with the XRD analysis (Fig. 2).

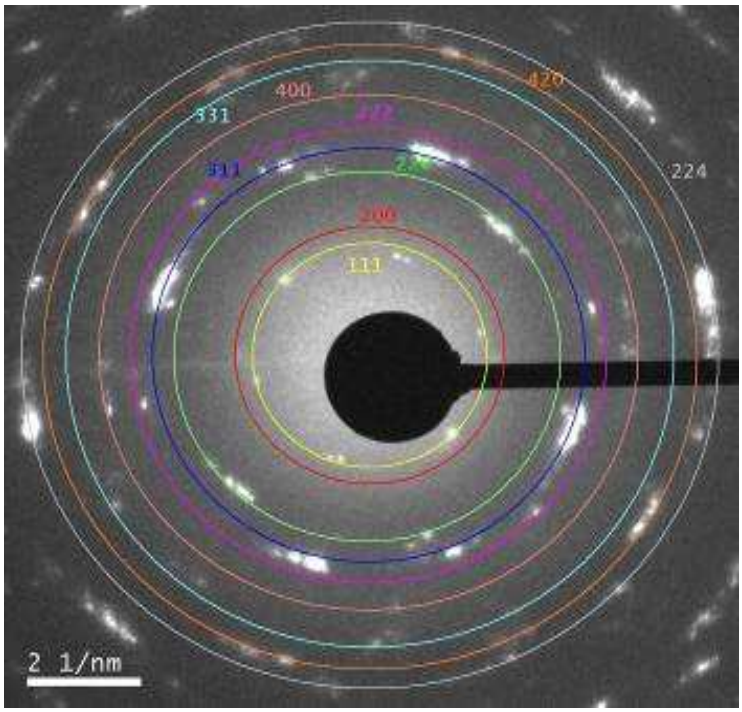

Fig. 5: Diffraction pattern from agglomerate. The ring sequence corresponds to the cubic lattice.

E. Temperature Program Reduction (TPR)

TPR experiments were conducted for $Mn_{0.8}Zn_{0.2}Fe_2O_4$ (Fig. 6). Experiments were carried out at a heating rate of 5°C/min. The reactive gas composition is hydrogen (5 vol %) in nitrogen. The flow rate was fixed at 20 ccm/min. The total reactive gas consumption during TPR analysis was measured. The TPR measurement was carried out following activation after cooling the sample in nitrogen flow to 40°C. Sample was then held at 1000°C for 10 min. The TPR experiment was performed at 800°C.

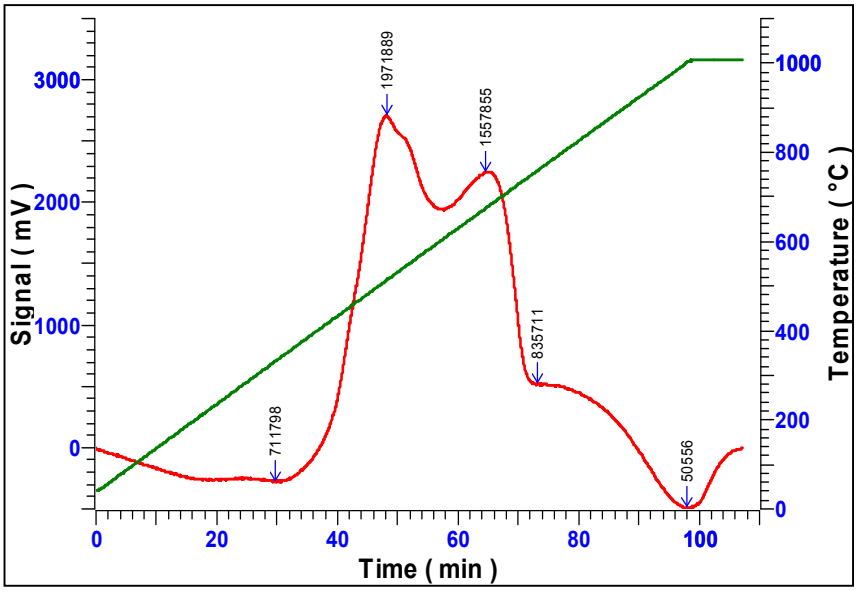

Fig. 6: Temperature program reduction profile for $Mn_{0.2}Zn_{0.8}Fe_2O_4$ annealed at 700°C, for 4 hours.

Referring to Fig. 6, the first reduction occurs at 331°C for Fe_2O_3 to Fe_3O_4. It has been reported that the reduction of Fe_2O_3 to Fe_3O_4 occurred at 350°C [11]. Other researchers found that it occurred at 370°C [12]. The second reduction peak for $Mn_{0.8}Zn_{0.2}Fe_2O_4$ is at 513°C. It can be speculated as a

reduction peak to MnO and FeO. It was reported that the second reduction peak occurred at 500°C – 600°C and at 540°C ferrite will reduce into FeO and MnO [12]. The third reduction peak is at 759°C which is an expected reduction temperature for all the oxide to the metallic state. $Mn_{0.8}Zn_{0.2}Fe_2O_4$ needs less energy activation to reduce to Mn and Fe metallic because the present of Mn that facilitates the reduction of Fe_2O_3 [11,12,13].

Table III. Data TPR for Mn¬0.8Zn0.2Fe2O¬ sintered at 700°C.

Temperature (°C)	% Hydrogen	mVs	µmol/g
331	13.88	711798.36	411.06086
513	38.45	1971888.74	1138.75830
675	30.38	1557855.31	899.65554
759	16.30	835710.65	482.61974
1002	0.99	50556.42	29.19614

Referring to Table III, it can be observed that the higher hydrogen uptake occurs at 513°C (38.45%) and 675°C (30.38%). From the experiment it can be observed that almost all the reduction process has occurred at 1000°C with only 0.99% hydrogen consumed.

F. Kjeldahl Method

The method to calculate the amount of ammonia produced is named Kjeldahl method [14,15].

$$NH_3 + HCl \rightarrow NH_4Cl$$
$$HCl_{reaction} + NH_3 \rightarrow NH_4Cl$$
$$NaOH + HCl_{excess} \rightarrow NaCl + H_2O$$
$$\text{Amount of } HCl_{reacted} = \text{Amount of } NH_3$$
$$\text{Amount of } HCl_{excess} = \text{Amount of NaOH}$$

Ammonia synthesis was done by diluting the gas to 5ml of 0.01M HCl which produced NH_4Cl. After that, the titration process was done by using 0.01M NaOH. The amount of NH_3 produced is equal to the amount of $HCl_{reaction}$.

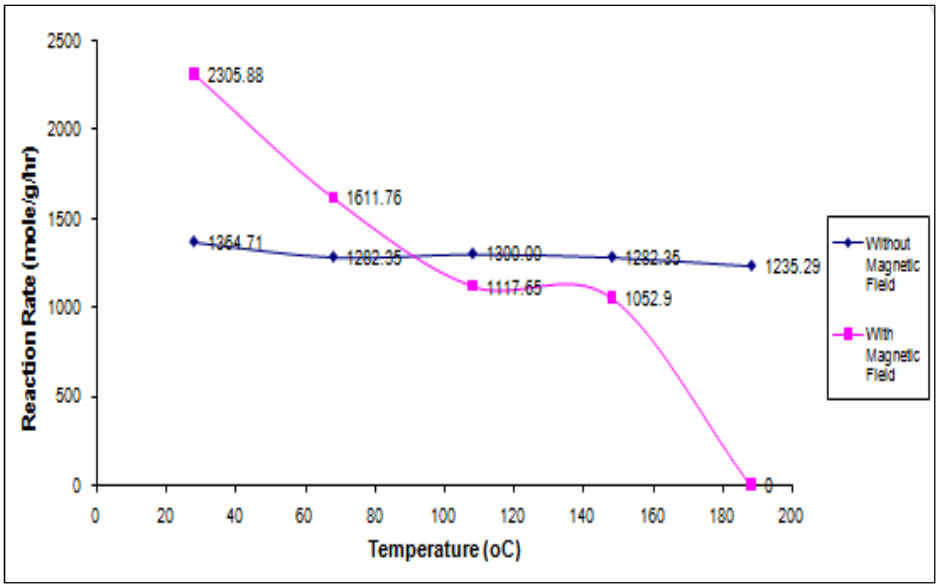

Fig. 7: Reaction Rate of Ammonia Production.

Fig. 7 shows the result of ammonia production conducted with and without magnetic induction. This reaction was done with the aid of $Mn_{0.8}Zn_{0.2}Fe_2O_4$ nanocatalyst which was synthesized at 700°C using the sol gel method. The ammonia production hardly changes when the reaction was done without magnetic induction at a temperature ranging from room temperature to 200°C. We invoke the influence of magnetic induction on the magnetic nanocatalyst leading to production of ammonia gas. Thermal agitation will be increased with the rise of temperature resulting to weakening of directionality of the moments and hence a steady decrease of the net magnetic moments. The more immediate observation is the yield of ammonia gas decreases with increasing temperature. Evident by the results in Fig. 7, we now offer a new approach of ammonia synthesis using magnetic induction.

G. Activation Energy

The activation energy was determined by the Arrhenius plot as shown in Fig. 8. Well known equations for ammonia synthesis namely Van't Hoff and Temkin-Phyzev were referred [16] and the calculations are described in Table IV.

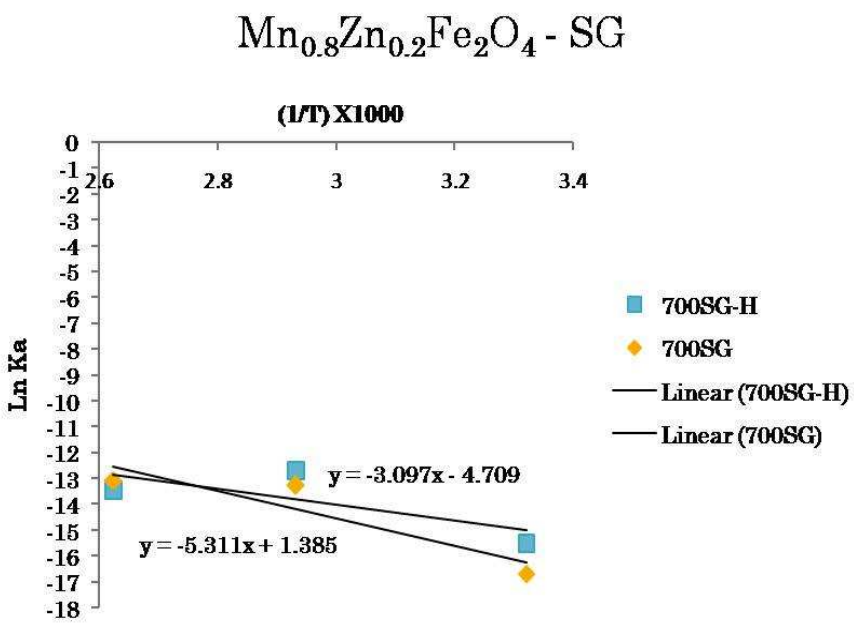

Fig. 8: Arrhenius plot of ammonia production for $Mn_{0.8}Zn_{0.2}Fe_2O_4$-SG nanocatalysts. T = 30°C-190°C, P = 1 atm, H-F = 1 T, Cat. = 0.2 g, GHSV = 12000 $cm^3/g_{cat}.h$, F = 40 cm^3/min, H_2:N_2 = 3:1.

The activation energy can be obtain by using the equation:

$$k = Ae^{\left(\frac{-Ea}{RT}\right)}$$

where,
Ea = the activation energy, R = 8.314 x 10-3 kJ $mole^{-1}$ K^{-1},T = temperature in Kelvin and A = proportionality constant.
Taking the natural logarithm of Arrhenius equation [17] gives,

$$\ln(k) = -\frac{Ea}{R}\Big) x \left(\frac{1}{T}\right. + \ln(A)$$

$$Y = mx + c$$

Plot ln(k) vs $\frac{1}{T}$ and the data will give a straight line and by determining the slope, the value of activation energy can be calculated.

Table IV. Data to determine the activation energy

Material	T (^{o}C)	Mole (μ)	Rate (x10^{-4})	Keq	Ka (x10^{-8})	ln Ka	(1/T)x 1000
$Mn_{0.8}Zn_{0.2}Fe_2O_4$ with H-Field	28	39.2	3.92	237000	18.9	-15.48	3.32
	68	27.4	2.74	3090	307	-12.69	2.93
	108	19	1.90	87.64	144	-13.45	2.63
$Mn_{0.8}Zn_{0.2}Fe_2O_4$ Without H-Field	28	23.20	2.32	237000	0.06	-16.67	3.32
	68	21.80	2.18	3090	1.72	-13.27	2.93
	108	22.10	2.21	87.64	2.11	-13.07	2.62

The activation energy, E_a was determined by calculating the gradient of the linear lines (Fig. 8). In the absence of magnetic field, the $Mn_{0.8}Zn_{0.2}Fe_2O_4$ nanocatalyst had an activation energy of -44.16 kJ/mole. In the presence of magnetic field, the Ea of the $Mn_{0.8}Zn_{0.2}Fe_2O_4$ nanocatalyst was -25.70 kJ/mole. The Ea values for the nanocatalyst with the presence of magnetic field is lower than the nanocatalyst in the absence of magnetic field. This is because the nanocatalyst needs a lot of energy to release nitrogen and hydrogen in the absence of the magnetic field. Whereas, the reaction with the presence of magnetic field required less energy to release the hydrogen and nitrogen because the spin alignment will enhance the ability of the nanocatalyst to obtain the higher yield of ammonia. Both reactions are exothermic and this is according to the theory of ammonia synthesis by the Haber Bosch process. The activation energy of Pd/SiO_2 catalyst was 27.7 kcal/mol at 500^{o}C and it was dropped by the presence of Ag [18]. Other researcher found that the activation energy of Ni-based catalyst for methane production was 90.9, 111.8, 79.5, and 85.9 kJ/mol, respectively [19]. By the presence of a magnetic field, the activation energy of catalyst can be reduced since the reaction take place at room temperature. It can be concluded that magnetizing the catalyst minimized the difficulty of electron exchanging and pairing process between catalyst and the reactant gas.

Conclusion

The new nanocatalysts from $Mn_{0.8}Zn_{0.2}Fe_2O_4$ has been used for ammonia synthesis. In the presence of a magnetic field, the activation energy is 30% lower than without the presence of magnetic field. The excellent ammonia yield (46%) successfully achieved at room temperature (28^{o}C) and ambient pressure in the applied magnetic field (1 Tesla). Room temperature and ambient pressure are the most conducive environments to synthesis ammonia because it is easy to control, safe and cost effective.

Acknowledgement

The authors acknowledge the Ministry of Science and Technology Malaysia for the E-Science research fund (code 03-02-02-SF0031). Dr Koziol thanks the Royal Society for funding.

References

[1] N. Yahya, Ammonia Synthesis, Carbon and Oxide Nanostructures, Springer, Germany, 2010, 395-413.
[2] R.E. Calderón Ortiz. Master Thesis. University of Puerto, 2008.
[3] C.M. Roebuck Exeel HSC Publisher (1008) 35-41.
[4] K.N. Whitten, R.E. Davis, M.L Peck, G.G. Stanley, Thomson Brookscole 7 (2003) 813-720.
[5] G.A. Somorjai, Introduction to surface chemistry and catalysis, Wiley, USA (1994) 452-454.
[6] N. Yahya, P. Puspitasari, K. Koziol, N. Zabidi, M. Othman, International Journal of Engineering 1 (2010) 10-14.
[7] S.M. Yunusov, E.S. Kalyuzhnaya, B.L. Moroz, A.S. Ivanova, T.V. Reshtenko, L.B. Avdeeva, V.A. Likholobov, V.B. Shur, Journal of Molecular Catalysis A: Chemical 219 (2004) 149-153.
[8] Labconco, An Industry Service Publication.
[9] D. Le Roux, F. Onno and P. Perriat, Proceeding ICF-5 (1989) 95-102.
[10] M.M. Rashad, Materials Science and Engineering B 127 (2006) 123–129.
[11] A. Khan, Panagiotis G. Smirniotis, Journal of Molecular Catalysis A: Chemical 280 (2008) 43-51.
[12] L.C.A Oliveira, J.D Fabris, R.R.V.A. Rios, W.N. Mussel, R.M. Lago, Applied Catalyst A: General 259 (2004) 253-359.
[13] G. Flavia D, Bibiana P. Barbero, Luis E. Cadius, C. Rojas, A. Centeno, A. Odrizola, Applied Catalyst B: Environmental 92 (2009) 194-201.
[14] F. Trachsel, C. Hutter, Phillip R. von Rohr, Chemical Engineering Journal 135S (2008) 309-316.
[15] J. Park, K. B. Park, K.S. Shin, H. D. Park, M.C. Kim, J. R. Kim, S. N. Park, Y. H. Song, Sensors and Actuators B: Chemical 117 (2006) 516-522.
[16] S.E. Nielsen. Ammonia Synthesis: Catalyst and Technologies. American Chemical Society, Chapter 2, (2008) 15-39.
[17] S. Arrhenius, Z. Phys. Chem 4 (1889) 226-248.
[18] H. Zea, K. Lester, A.K. Datye. E. Rightor, R. Gulotty, W. Waterman, M. Smith, Applied
Catalyst A: General 282 (2005) 237-245.
[19] C. Yuehua, X. Hengyong, G.E. Qingjie, W. Yuzhong, H. Shoufu, L. Wenzhao, Chinese Journal of Catalysis 27 (2006) 479-484.